2023 IEEE/ASME INTERNATIONAL CONFERENCE ON ADVANCED INTELLIGENT MECHATRONICS (AIM)

AFM Microcantilever with On-chip Electrothermal and Piezoelectric Transducers: Z-axis Control and Standalone Operation

Hazhir Mahmoodi Nasrabadi, Nastaran Nikooienejad, K. S. Vikrant, S. O. Reza Moheimani, *Fellow, IEEE,*

***Abstract*—The Atomic Force microscope (AFM) has limited throughput, which is a major obstacle to its widespread industrial application. This is due to the conventional imaging technique where a single AFM probe interacts with each point on a sample sequentially. In this paper, we propose a solution to this problem by introducing an array of three active microcantilevers that can operate in parallel. Although all three microcantilevers can be used for imaging, in this work, we only report imaging with the central microcantilever, while the other two are held at a fixed height above the sample. Each microcantilever has on-chip piezoelectric and electrothermal actuators that provide high-frequency and large-range Z-motion to the tip, respectively. The deflection of the tip during imaging is measured by an on-chip differential piezoelectric sensor, and the topography of the sample is determined by controlling the deflection. We microfabricated the array of microcantilevers and integrated them with an in-house developed AFM set-up to image several calibration gratings. This work lays the foundation for the parallel operation of multiple AFM probes, which can significantly improve the throughput of AFM in industrial applications.**

***Index Terms*—Active AFM Microcantilever, Piezoelectric Sensing/Actuation, Electrothermal Actuation, Z Positioner, Feedback Loop**

I. Introduction

THE Atomic Force Microscope (AFM) has been widely used in scientific research for four decades. It can be used for imaging, characterization, manipulation, and fabrication of micro and nanoscale samples in different environments, from ambient to ultrahigh vacuum. AFM can be applied to various materials regardless of their electrical conductivity [1]. There are three major modes for AFM: contact [2], noncontact [3], [4], and tapping mode [5], [6], [7].

In all three modes, AFM uses a micromachined cantilever with a sharp tip to interact with samples, with forces regulated by feedback control. In tapping mode, forces are measured by cantilever deflection and regulated using a Z-actuator, also known as Amplitude Modulation AFM (AM-AFM) [8], [9]. Scanning the sample changes the oscillation amplitude, reflecting the sample topography in the controller output, which compensates for the deflection change.

The classic microcantilever displacement sensing method used an optical beam deflection (OBD) measurement system, where a laser-light is focused on the cantilever's back, and a four-quadrant photodiode surface collects the reflected light to generate the displacement signal [10]. While precise, this method and the base shaker actuator used in classic AFM setups increase the device's footprint, making it susceptible to vibration and limiting parallel imaging for high throughput inline metrology. Aligning the optical sensing system is also time-consuming [9], [11], and the base shaker excitation can introduce complex dynamics and distortions, causing inaccuracies in system identification [12].

To reduce the footprint of the AFM setup, researchers have developed methods based on microelectromechanical systems (MEMS) actuation and sensing mechanisms to implement the actuator and the sensor on the cantilever chip. On-chip actuation uses physical phenomena such as piezoelectric, electrothermal, or electrostatic methods to deflect the cantilever, while on-chip sensing translates cantilever deflection to a physical quantity using methods such as piezoelectric, piezoresistive, or electrostatic techniques [13], [14], [15], [16]. However, introducing on-chip actuation and sensing can result in some feedthrough to the system due to the adjacency of the actuation and sensing terminals and tracks in active AFM microcantilevers. This feedthrough can be eliminated using various methods [17], [18], [19].

An active AFM microcantilever's low footprint makes it ideal for array AFM imaging [7]. An on-chip Z-axis positioner is required for independent control of each cantilever in the array. Ahmad et al. [20] presented an array of active AFM microcantilevers capable of Z-axis positioning using an electrothermal actuator and an integrated piezoresistive sensing mechanism. The high displacement of electrothermal actuation makes it suitable for Z-axis control, but the piezoresistive sensor is sensitive to the high-temperature behavior of the actuator [21].

This article presents a novel method that uses a piezoelectric actuator for high-frequency cantilever actuation and an electrothermal actuator for the Z-positioning of the tip. To overcome the temperature sensitivity issue of the piezoresistive sensor, a piezoelectric sensor is used instead, which is easier to microfabricate. The paper comprises three sections, which discuss the design of the device, characterization of actuation and sensing mechanisms, and AFM imaging, followed by a conclusion.

II. Design

The microcantilever is designed to have a stepped rectangular geometry that includes a wider and a smaller rectangular sections of dimensions $\sim 300 \times 300\,\mu\text{m}^2$ and $\sim 200 \times 70\,\mu\text{m}^2$, respectively (Fig. 1(a)). The wider rectangular section comprises three laterally symmetric piezoelectric elements wherein the

Corresponding Author: S. O. Reza Moheimani (Reza.Moheimani@utdallas.edu).

Manuscript is submitted to 2023 IEEE/ASME International Conference on Advanced Intelligent Mechatronics (AIM)

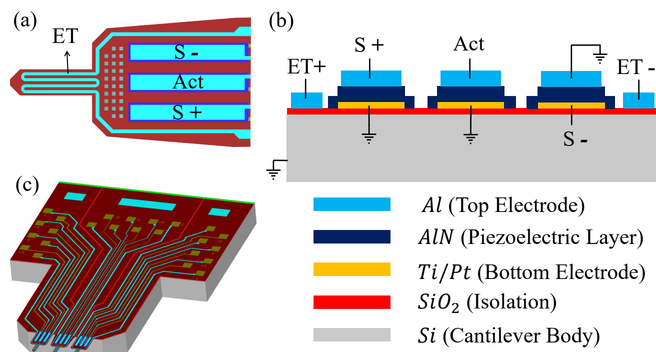

Fig. 1: structure of the cantilever

central element forms the actuator and the two side elements form the sensor. The symmetrical lateral placement of the three transducer elements results in a collocated actuator-sensor system which provides robust stability to the closed-loop system. Although the piezoelectric actuator can provide high-frequency motion, the thermal actuators have the advantages of low-voltage operation and large forces compared to other MEMS actuation mechanisms [22], [23]. Therefore, an electrothermal actuator that can provide a relatively larger Z-motion range is employed by designing a serpentine aluminum track on the smaller rectangular section.

The cross-sectional view in Fig. 1(b) shows the electrical connections for the piezoelectric actuator, electrothermal actuator, and piezoelectric sensor. The electrical connections were used to apply and measure the voltage across the actuation and sensing elements, respectively. The applied voltages to the actuators generate strain and hence provide Z-motion to the microcantilever. The dynamic Z-motion of the microcantilever strains the sensing elements resulting in charge generation across the faces of the sensing elements. It is worthwhile to note that the electrodes S+ and S- are placed on opposite faces of the sensing elements, which results in strains with 180° phase difference.

This electrode configuration results in charges with opposite polarity, leading to a larger measurement signal when interfaced with the voltage amplifier. The designed microcantilever has independent actuation and sensing capabilities, allowing for several cantilevers to be fabricated on the same base, resulting in a low-footprint system. Fig. 1(c) shows an array of three identical microcantilevers designed with distinct resonance frequencies to reduce coupling between them. Additionally, the device layer of each cantilever has been isolated to prevent direct mechanical connection via the device layer [7].

III. Characterization

The actuation and sensing parameters of the fabricated microcantilever are experimentally obtained. Under actuation parameters, we measure the actuation gain and bandwidth of the microcantilever for both piezoelectric and electrothermal actuators. Under sensing parameters, we calculate the measurement sensitivity of the piezoelectric sensor.

First, we measure the actuation gain and resonant frequency of the microcantilever corresponding to piezoelectric actuation. Since piezoelectric actuation is employed for generating high-frequency oscillation, the actuation gains are measured only at high frequencies. Here a sinusoidal voltage of amplitude $100\,$mV is applied across the on-chip piezoelectric actuator and the frequency of the applied voltage is swept from $20\,$kHz to $70\,$kHz. The displacement at each frequency is measured using the on-chip piezoelectric sensor and a laser Doppler vibrometer (LDV). These measurements are employed to calculate the frequency response of the microcantilever as shown in Fig. 2. To better compare the FRF results, the magnitude at resonance for both responses is scaled to unity (0 dB). The peak of the piezoelectric sensor FRF is $-13.06\,$dB(V/V) and the FRF peak of the LDV is $-114.8\,$dB(m/V). The plots show that the resonance frequency of the cantilever is $44.69\,$kHz and the actuation gain near the resonance frequency is $1.85\,\mu$m/V. Furthermore, the plots also reveal that the measurement sensitivity of the piezoelectric sensor remains almost constant at $1.22\,$V/μm near the resonance frequency. We also observe that the piezoelectric response follows the model response captured in LDV. This reveals that the feedthrough between the on-chip actuator and the sensor has been effectively canceled owing to the differential sensing technique.

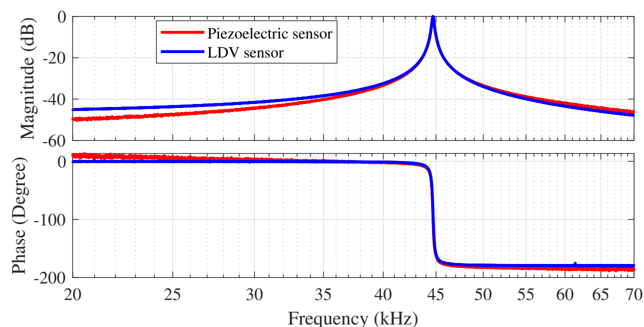

Fig. 2: Frequency response of the open-loop piezoelectric actuation. The deflection sensing is performed by the on-chip piezoelectric sensor (red line) and a laser Doppler vibrometer (LDV) sensor (blue line). The magnitudes at resonance are scaled to unity (0 dB) for better comparison.

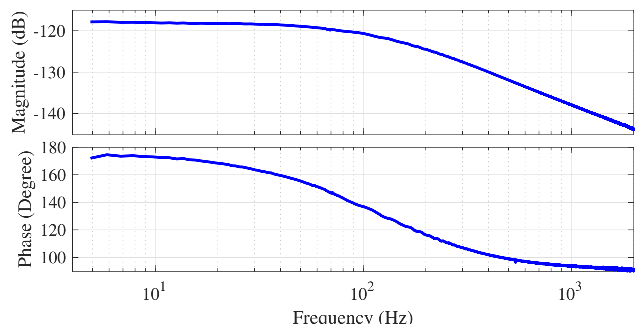

Fig. 3: The frequency response of the open-loop electrothermal system.

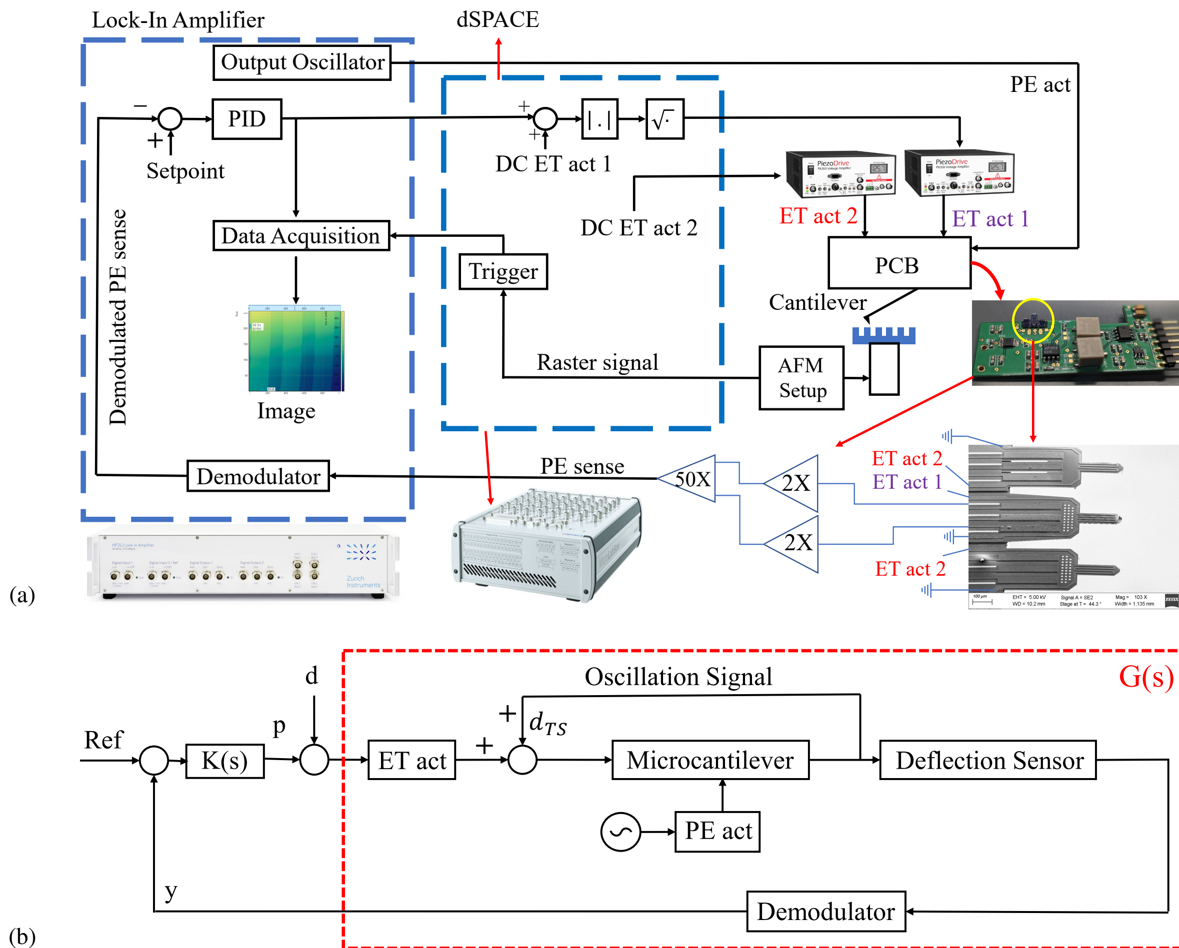

Fig. 4: (a) Feedback loop for tapping mode AFM imaging using off-the-shelf equipments. (b) Simplified schematic of the feedback loop.

Next, the actuation gain and bandwidth of the microcantilever corresponding to electrothermal actuation are determined. In the electrothermal actuator, the generated power will expand the Al layer, which results in a bimorph displacement in the Z direction. The displacement is proportional to the generated power, which is proportional to the $v^2(t)$. This non-linear nature of the electrothermal actuator necessitates a linearization of the electrothermal actuation voltage, which is realized by performing a $sqrt(.)$ function on the absolute value of the actuation voltage. Also, the electrothermal actuation only increases the temperature, which results in only expansion and not compression. Therefore, electrothermal actuation only deflects the cantilever in one direction. To achieve bi-directional deflection, a constant voltage is applied across the electrothermal actuator which keeps the cantilever in a mean deflected position. Subsequently, when an additional AC voltage is added, the cantilever deflects up and down from its initial mean position for positive and negative cycles of the applied AC voltage, respectively.

From the experiments, we conclude that our devices are capable of producing approximately 10 μm Z deflection, which is enough for the sample profile and system drift. The electrothermal actuation should have a bandwidth greater than the highest spatial bandwidth to follow the sample profile. The actuation voltage is initially linearized in a dSPACE rapid prototyping system. In order to generate enough current (around 100 mA), a high-current amplifier is used in the path. Fig. 3 shows the frequency response of the open-loop electrothermal system (including the linearization block, the amplifier, and the on-chip electrothermal actuator) to a periodic chirp actuation voltage with AC amplitude of 1 V added to 1 V DC voltage. The actuator behaves as a first-order system with a cut-off frequency of approximately 100 Hz. Thus, the spatial imaging bandwidth is constrained by the 100 Hz electrothermal actuation bandwidth.

IV. Closed Loop System and AFM Imaging

As a proof of concept, the imaging is performed only by the array's middle cantilever. The other adjacent cantilevers are lifted using their on-chip electrothermal actuation to avoid any undesired contact with the sample (ET act 2 signal in Fig. 4(a)). The LIA applies a sine voltage with 65 mV amplitude at the resonance frequency of the cantilever before the tip-sample

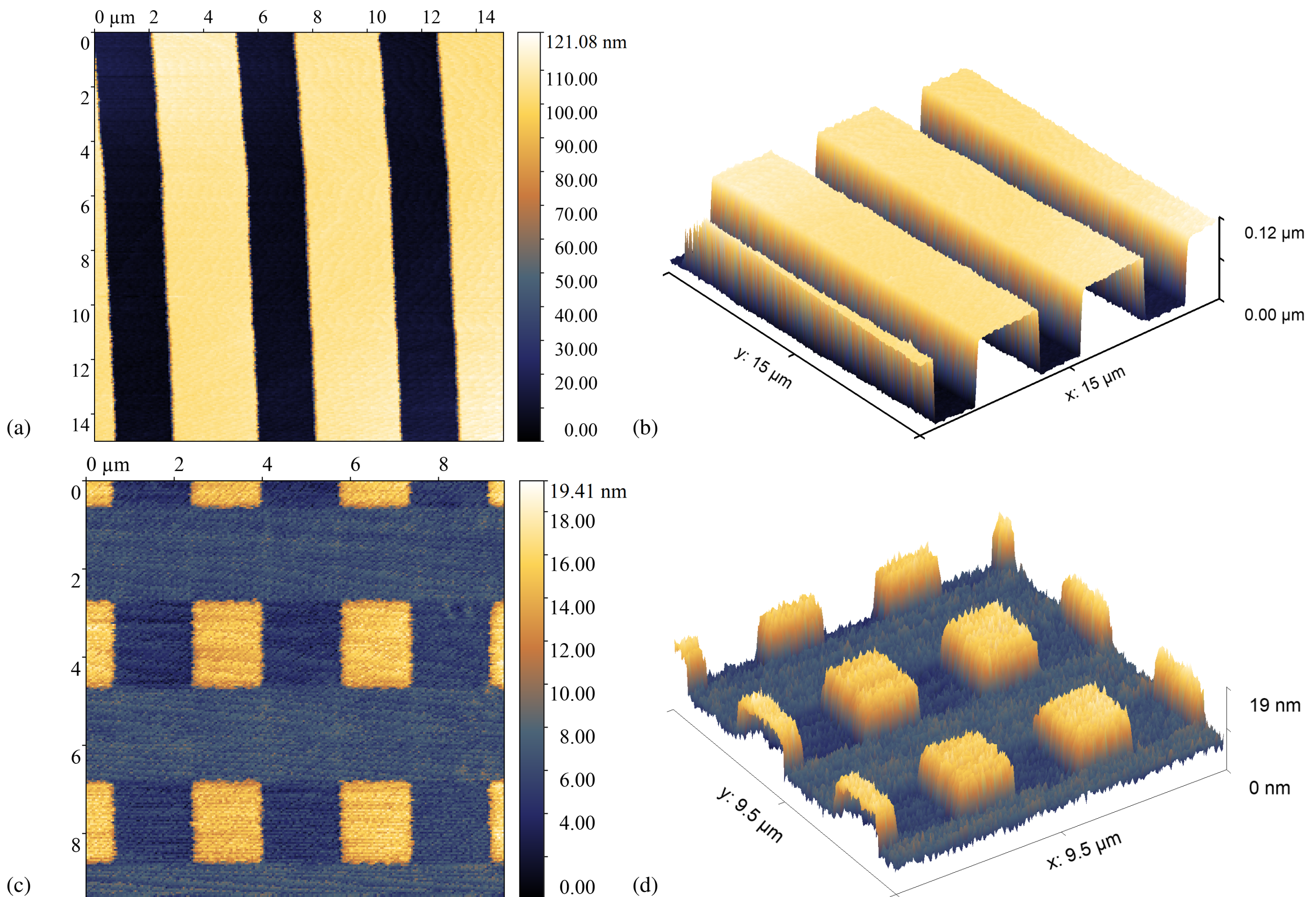

Fig. 5: AFM images of three calibration gratings with a scan rate of $1\,row/s$. The imaging is in ambient condition. (a),(b) 2D and 3D images of a calibration grating with step heights of $114\,$nm and a period of $5\,\mu$m (model: HS-100MG), respectively; (c),(d) 2D and 3D images of a calibration grating with step heights of $20\,$nm and a period of $3\,\mu$m (model: TG3D-3000/20), respectively; The features obtained in the AFM images match the specifications provided by the manufacturer of the gratings and the data obtained by the traditional AFM process.

approach. This actuation results in $120\,$nm tip displacement in free air. The sensing signals are differentially amplified and passed to the LIA for demodulation. The free air deflection results in $140\,$mV demodulated sensing signal (see Fig. 4).

To enable bidirectional deflection, a DC voltage is applied to the electrothermal actuator. The cantilever's resonance frequency shifts a few hertz due to the resulting heat. The resonance frequency is additionally shifted by several hertz due to the heat produced by the electrothermal actuator of the adjacent cantilevers. The actuation frequency is then adjusted to compensate for these shifts in frequency. Once the transient thermal effects of the electrothermal actuators settle down and the entire system reaches a steady state temperature, the tip of the microcantilever is docked on the sample using the conventional tip-approach procedure. The docking of the tip on the sample results in a reduced oscillation amplitude due to the energy losses associated with the intermittent contact. Since we are imaging hard samples, we select an oscillation amplitude that is 60% of the free air amplitude ($\sim 72\,$nm). Since the commercial AFM tip-approach mechanism is used to land the cantilever, a slider gain is employed in dSPACE to gradually increase the PI gains to $\mathrm{P} = 1$ and $\mathrm{I} = 1000$ in the HF2LI and replace the piezo Z actuator of the AFM setup with the on-chip electrothermal actuator in the feedback loop. The selected proportional-integral controller ensures that the closed-loop system has sufficient phase and gain margins and remains stable during AFM imaging.

The imaging process is performed on 2 different calibration gratings (Fig. 5). The trigger signal generated in the dSPACE using the rastering signal of the AFM setup is used to measure the X and Y data of each pixel of the image, and the controller output is the Z data of each pixel. The X, Y, and Z information of each pixel is saved in the DAQ tab of the HF2LI and are used to create the final 2D and 3D images of each sample. For the first AFM image (Fig. 5.(a),(b)), an area of $15\,\mu\text{m} \times 15\,\mu$m is swept. The calibration sample features trenches with $114\,$nm

height and a period of $3\,\mu$m. The second AFM imaging (Fig. 5.(c),(d)) is performed on a calibration sample with square-shaped features with the height of $18\,$nm and period of $3\,\mu$m, in an area of $9.5\,\mu$m × $9.5\,\mu$m. Fig. 5.

V. Conclusion and Future Research

This article presented the design, development, and evaluation of three parallel active microcantilevers with independent Z-actuation and sensing capability. The microcantilever's design uses a novel combination of on-chip electrothermal and piezoelectric actuators and an on-chip piezoelectric sensing technique. The microcantilevers with on-chip actuators and sensors were fabricated using a Silicon batch processing technique and a tip was integrated at the extremity of the middle cantilever. Next, the natural frequency and actuation gain for the middle microcantilever was characterized. Subsequently, the chip was integrated into an in-house developed AFM, which was instrumented with the necessary drivers, the data acquisition system, and the sample positioning stage. Finally, tapping mode AFM imaging was demonstrated by imaging 2 standard AFM calibration gratings using only the middle microcantilever.

In future work, first, the closed-loop system identification will be presented. Then, simultaneous AFM imaging with multiple cantilevers to increase the throughput will be demonstrated. One possible challenge will be to ensure that the surfaces of the micro-cantilevers and the sample surface are co-planar so that the tip on each cantilever can interact with the sample. This issue can be resolved by mounting the sample on a tilting stage.

Acknowledgments

The authors would like to thank the staff of the cleanroom at the University of Texas at Dallas for providing the tools for the microfabrication process.

This work was supported by the U.S. Department of Energy's Office of Energy Efficiency and Renewable Energy (EERE) under the Advanced Manufacturing Office Award No. DE-EE0008322, and the UT Dallas Center for Atomically Precise Fabrication of Solid-State Quantum Devices.

References

1 M. Z. Baykara and U. Schwarz, "Atomic force microscopy: Methods and applications," in *Encyclopedia of spectroscopy and spectrometry*, Elsevier, 2017.

2 G. Schitter, R. Stark, and A. Stemmer, "Fast contact-mode atomic force microscopy on biological specimen by model-based control," *Ultramicroscopy*, vol. 100, no. 3-4, pp. 253–257, 2004.

3 F. J. Giessibl, "The qPlus sensor, a powerful core for the atomic force microscope," *Review of Scientific Instruments*, vol. 90, no. 1, p. 011101, 2019.

4 E. I. Altman, M. Z. Baykara, and U. D. Schwarz, "Noncontact atomic force microscopy: an emerging tool for fundamental catalysis research," *Accounts of Chemical Research*, vol. 48, no. 9, pp. 2640–2648, 2015.

5 O. Kaveh, M. B. Coskun, M. Mahdavi, and S. O. R. Moheimani, "Fpga-based characterization and q-control of an active AFM cantilever," in *2020 IEEE/ASME International Conference on Advanced Intelligent Mechatronics (AIM)*, pp. 2062–2067, IEEE, 2020.

6 M. B. Coskun, H. Alemansour, A. G. Fowler, M. Maroufi, and S. O. R. Moheimani, "*Q* control of an active AFM cantilever with differential sensing configuration," *IEEE Transactions on Control Systems Technology*, vol. 27, no. 5, pp. 2271–2278, 2018.

7 M. B. Coskun, M. Baan, A. Alipour, and S. O. R. Moheimani, "Design, fabrication, and characterization of a piezoelectric AFM cantilever array," in *2019 IEEE Conference on Control Technology and Applications (CCTA)*, pp. 227–232, IEEE, 2019.

8 H. Mahmoodi Nasrabadi, M. Mahdavi, M. Soleymaniha, and S. O. R. Moheimani, "High resolution atomic force microscopy with an active piezoelectric microcantilever," *Review of Scientific Instruments*, vol. 93, no. 7, p. 073706, 2022.

9 M. W. Fairbairn and S. O. R. Moheimani, "Control techniques for increasing the scan speed and minimizing image artifacts in tapping-mode atomic force microscopy: Toward video-rate nanoscale imaging," *IEEE Control Systems Magazine*, vol. 33, no. 6, pp. 46–67, 2013.

10 D. Rugar and P. Hansma, "Atomic force microscopy," *Physics today*, vol. 43, no. 10, pp. 23–30, 1990.

11 M. G. Ruppert and S. O. R. Moheimani, "High-bandwidth multimode self-sensing in bimodal atomic force microscopy," *Beilstein journal of nanotechnology*, vol. 7, no. 1, pp. 284–295, 2016.

12 M. Dukic, J. D. Adams, and G. E. Fantner, "Piezoresistive AFM cantilevers surpassing standard optical beam deflection in low noise topography imaging," *Scientific reports*, vol. 5, no. 1, pp. 1–11, 2015.

13 A. Onaran, M. Balantekin, W. Lee, W. Hughes, B. Buchine, R. Guldiken, Z. Parlak, C. Quate, and F. Degertekin, "A new atomic force microscope probe with force sensing integrated readout and active tip," *Review of Scientific Instruments*, vol. 77, no. 2, p. 023501, 2006.

14 A. Buguin, O. Du Roure, and P. Silberzan, "Active atomic force microscopy cantilevers for imaging in liquids," *Applied Physics Letters*, vol. 78, no. 19, pp. 2982–2984, 2001.

15 N. F. de Bem, M. G. Ruppert, Y. K. Yong, and A. J. Fleming, "Integrated force and displacement sensing in active microcantilevers for off-resonance tapping mode atomic force microscopy," in *2020 International Conference on Manipulation, Automation and Robotics at Small Scales (MARSS)*, pp. 1–6, IEEE, 2020.

16 M. Soleymaniha, M. B. Coskun, H. M. Nasrabadi, A. Alipour, and S. O. R. Moheimani, "Design, fabrication and characterization of active atomic force microscope cantilever arrays," in *2021 IEEE 34th International Conference on Micro Electro Mechanical Systems (MEMS)*, pp. 883–886, IEEE, 2021.

17 M. B. Coskun, A. G. Fowler, M. Maroufi, and S. O. R. Moheimani, "On-chip feedthrough cancellation methods for microfabricated AFM cantilevers with integrated piezoelectric transducers," *IEEE Journal of Microelectromechanical Systems*, vol. 26, no. 6, pp. 1287 – 1297, 2017.

18 M. Mahdavi, M. B. Coskun, H. M. Nasrabadi, and S. O. R. Moheimani, "A high dynamic range AFM probe with collocated piezoelectric transducer pairs," in *The 33rd IEEE International Conference on Micro Electro Mechanical Systems (MEMS 2020)*, 2020.

19 M. G. Ruppert, S. I. Moore, M. Zawierta, A. J. Fleming, G. Putrino, and Y. K. Yong, "Multimodal atomic force microscopy with optimized higher eigenmode sensitivity using on-chip piezoelectric actuation and sensing," *Nanotechnology*, vol. 30, no. 8, p. 085503, 2019.

20 A. Ahmad, N. Nikolov, T. Angelov, T. Ivanov, A. Reum, I. Atanasov, E. Guliyev, V. Ishchuk, M. Kaestner, Y. Krivoshapkina, *et al.*, "Large area fast-AFM scanning with active "quattro" cantilever arrays," *Journal of Vacuum Science & Technology B, Nanotechnology and Microelectronics: Materials, Processing, Measurement, and Phenomena*, vol. 34, no. 6, p. 06KM03, 2016.

21 M. Maroufi, A. Bazaei, A. Mohammadi, and S. O. R. Moheimani, "Tilted beam piezoresistive displacement sensor: Design, modeling, and characterization," *Journal of Microelectromechanical Systems*, vol. 24, no. 5, pp. 1594–1605, 2015.

22 Y. Zhu, A. Bazaei, S. O. R. Moheimani, and M. R. Yuce, "A micromachined nanopositioner with on-chip electrothermal actuation and sensing," *IEEE Electron device letters*, vol. 31, no. 10, pp. 1161–1163, 2010.

23 V. Kaajakari, *Practical mems*. Small Gear Publishing Las Vegas, 2009.